

Research Article

Open Access



# Disturbance observer-based terminal sliding mode control for the training safety improvement in robot-assisted rehabilitation

Yaqi Zhang, Weiyi Xie, Renjie Ma

College of Engineering, Shantou University, Shantou 515063, Guangdong, China.

**Correspondence to:** Yaqi Zhang, College of Engineering, Shantou University, 243 Daxue Rd., Jinping District, Shantou 515063, Guangdong, China. E-mail: yaqizhang103@163.com

**How to cite this article:** Zhang, Y.; Xie, W.; Ma, R. Disturbance observer-based terminal sliding mode control for the training safety improvement in robot-assisted rehabilitation. *Intell. Robot.* 2025, 5(2), 333-54. <http://dx.doi.org/10.20517/ir.2025.17>

**Received:** 11 Nov 2024 **First Decision:** 3 Jan 2025 **Revised:** 20 Feb 2025 **Accepted:** 25 Feb 2025 **Published:** 11 Apr 2025

**Academic Editor:** Jinhua She **Copy Editor:** Pei-Yun Wang **Production Editor:** Pei-Yun Wang

## Abstract

Existing control methods for exoskeletons often face challenges in adapting to individual differences, ensuring robustness in dynamic environments, and achieving real-time performance. For instance, certain approaches fail to balance rehabilitation efficacy with wearer comfort, while others suffer from issues such as chattering and limited disturbance rejection capabilities. This paper proposes a control framework for exoskeleton rehabilitation robots, emphasizing the strict implementation of safety protocols to guarantee that patients in the early stages of rehabilitation can accurately follow normal human activity postures. Firstly, an interpolating polynomial is optimized to generate the desired trajectory, with consideration of the minimum jerk principle. Secondly, a motion-dependent function is proposed for smooth switching between two modes of normal training and safe stopping. Thirdly, a non-singular fast terminal sliding mode method based on a nonlinear disturbance observer is proposed to accurately track the desired joint angles, with the objective of achieving a tracking error that tends to zero in a finite time. Furthermore, the stability of the closed-loop system is demonstrated through the application of the Lyapunov method. Ultimately, the simulation results demonstrate the efficacy and resilience of the proposed control framework.

**Keywords:** Non-singular terminal sliding mode control, disturbance observer, minimum-jerk, smooth switching, Lyapunov methods



© The Author(s) 2025. **Open Access** This article is licensed under a Creative Commons Attribution 4.0 International License (<https://creativecommons.org/licenses/by/4.0/>), which permits unrestricted use, sharing, adaptation, distribution and reproduction in any medium or format, for any purpose, even commercially, as long as you give appropriate credit to the original author(s) and the source, provide a link to the Creative Commons license, and indicate if changes were made.



## 1. INTRODUCTION

Stroke is recognized as the third leading cause of disability and death worldwide, according to the World Stroke Data Showcase<sup>[1]</sup>. The current global incidence of stroke has surpassed 15 million cases<sup>[2]</sup>. Furthermore, the number of new stroke cases each year is extremely large and shows a continuously increasing trend. The majority of stroke patients experience severe disabilities, predominantly motor movement disorders of the limbs, which significantly affect their daily living activities<sup>[3]</sup>. To promote functional recovery and prevent further deterioration, rehabilitation is considered crucial for these patients. The recovery of motor function in stroke patients mainly depends on early intervention and continuous rehabilitation training, including physical therapy (PT), occupational therapy (OT), and robot-assisted training. These methods aim to promote neural plasticity and functional reconstruction. Among them, repetitive training has been proven to be an effective means of enhancing muscle strength and improving motor control<sup>[4]</sup>. Compared with traditional PT and OT, robot-assisted movement training has shown significant advantages in clinical outcomes and biomechanical measurements, and its effectiveness in promoting the rehabilitation of stroke patients has been widely confirmed<sup>[5]</sup>. Robot-assisted training provides consistent and precise repetitive movements, allowing patients to perform high-intensity repetitive training, which is difficult to achieve in traditional PT and OT. This training method can provide mechanical assistance to the limbs, enabling patients to perform repetitive training of voluntary movements, which is of great help to patients who have difficulty moving automatically due to the aftermath of a stroke. As a nascent technology, robot-assisted training has demonstrated its distinctive merits in clinical and biomechanical assessments, providing new avenues for the rehabilitation of stroke patients<sup>[6,7]</sup>.

Due to the intimate physical interaction between exoskeletons and humans, motion planning is an essential component of exoskeleton control systems. Trajectory planning is not only related to the wearer's safety and comfort but also directly affects the effectiveness of rehabilitation training. Trajectory planning algorithms can be primarily divided into two major categories: Cartesian space trajectory planning and joint space trajectory planning. Cartesian space trajectory planning focuses on the motion trajectory of the end-effector in the Cartesian coordinate system, while joint space trajectory planning concentrates on the motion trajectory of the robot's individual joints in the joint space. Trajectories in the task space need to be converted from Cartesian coordinates to joint angles using inverse kinematics<sup>[8,9]</sup>, but it is difficult to obtain a non-unique solution for inverse kinematics in the human-machine workspace<sup>[10,11]</sup>. Optimization-based trajectory planning methods can systematically consider various performance indicators, such as time, energy consumption, and path length, in search of the theoretically optimal solution. Common optimization models include the minimum jerk model<sup>[12,13]</sup>, minimum torque model<sup>[14,15]</sup>, minimum inertia model<sup>[16,17]</sup>, minimum potential energy model<sup>[18,19]</sup>, etc. Wang *et al.* utilized an adaptive frequency oscillator (AFO) to extract high-level features from the active arm movement, then combined the motion rhythm with the principle of minimum jerk to generate an optimal reference trajectory, which is synchronized with the patient's movement intention and the movement patterns of healthy individuals<sup>[20]</sup>. Sampling-based methods<sup>[21,22]</sup>, such as rapidly-exploring random trees (RRT) and probabilistic roadmaps (PRM), are suitable for complex environments and high-dimensional spaces, capable of handling narrow or cluttered obstacle situations, but may require a large number of samples to ensure the feasibility of the path, leading to high computational costs. Machine learning-based techniques<sup>[23–26]</sup> and learning methods based on Hidden Markov Models (HMM) and Gaussian Mixture Models (GMM)<sup>[27]</sup> can learn from data and adapt to different tasks and user behaviors, but they require a substantial amount of training data, and their generalization capabilities for unseen situations may be limited.

The rehabilitation robot is designed to assist the patient in moving along a specific trajectory. The objective of the rehabilitation robot is to minimize tracking errors, thereby facilitating the patient's acquisition of normal movement patterns. This training modality is particularly well-suited for patients exhibiting impaired muscle movement during the pre-rehabilitation phase, as it serves to avert muscle atrophy. However, the implementation of passive rehabilitation training requires caution to ensure the safety of the patient and the effectiveness of the training. Therefore, the establishment of motion-restricted areas is particularly important in passive

rehabilitation training<sup>[28]</sup>. Firstly, the setting of motion-restricted areas is a key measure to protect patient safety. It can prevent excessive joint movement, avoiding potential injuries such as dislocation, sprains, or pain. Secondly, appropriate motion restrictions can promote the gradual recovery of neuromuscular function, activating the neuromuscular system through moderate stimulation. Additionally, different patients have different rehabilitation needs and movement capabilities. The establishment of motion-restricted areas can be adjusted according to the specific circumstances of the patient to provide personalized rehabilitation training programs. Concomitantly, the establishment of areas subject to movement restrictions facilitates therapists in closely monitoring patient responses during the training process, enabling timely adjustment or cessation of the training to prevent further injury. Therefore, it is necessary to flexibly switch between different modes of normal training and safe stopping in rehabilitation training. Li *et al.* proposed a hybrid control method, where the controller includes three working modes: resistance mode, assist mode, and restriction mode, and switches between the three different modes based on the tracking error performance of the controller output, allowing the working mode to be automatically adjusted according to the subject's movement performance<sup>[29]</sup>. Zhang *et al.* proposed a unified control framework, which consists of a mode controller capable of smooth switching between robot operation modes and a task controller adapted to different training needs<sup>[30]</sup>. By employing a motion-related controller with a switching function mode, it achieves seamless and smooth mode switching, ensuring the smoothness and safety of the training. Wu *et al.* designed a fuzzy proportional-integral-derivative (PID) controller for the proposed device<sup>[31]</sup>. Combining fuzzy control with PID control by adjusting the parametric PID parameters online according to the control deviation and the deviation change rate, the controller is able to provide quantifiable assistance for a specific patient based on the error-based self-tuning of the parameters, but it may lead to a decrease in the system control accuracy and deterioration of the dynamic quality. To improve accuracy, the number of quantization stages needs to be increased, which increases the amount of computation and the number of rules. Proietti *et al.* introduced a controller that adaptively varies the feedback gain and thus the modulation of the impedance on a task-by-task basis; however, it requires more accurate modeling of the system and still falls short of the problem of high-frequency unmodelled dynamics and measurement accuracy<sup>[32]</sup>.

Sliding mode control (SMC) is an efficient and robust control method that can be combined with the unified control framework to improve the performance and adaptability of the system. Conventional SMC systems are mainly based on linear sliding mode surface controllers (LMC), which are easy to implement but have long convergence times. The terminal SMC (TSMC) strategy<sup>[33]</sup> has been proposed as a solution to the fast response problem, aiming to drive the system state to a predefined target state within a finite time. However, in practice, the TSMC strategy faces the singularity problem; i.e., in some regions of the state space, the control inputs may require infinitely large values to maintain the desired sliding modes. This problem may lead to discontinuities in the control inputs, which in turn cause system chattering. In addressing this challenge, researchers have proposed two approaches: non-singularity TSMC<sup>[34]</sup> and non-singularity fast TSMC. These approaches offer a partial solution to the chattering problem by mitigating the effects of controller discontinuities. However, they do not fully resolve the chattering issue. Zou *et al.* proposed an improved TSMC manifold design, which not only ensures the finite-time stability of the system in both the arriving and sliding phases, but also, by reducing the chattering, improves the overall control performance<sup>[35]</sup>.

However, existing sliding surface designs primarily focus on attenuating matched disturbances. For mismatched disturbances - those that reside in different channels from the control input or whose directions do not align with the control input - direct compensation via the control input is not feasible. Instead, more sophisticated control strategies are required to address these disturbances. Mismatched disturbances are prevalent in various practical systems, and in such cases, the robustness of conventional SMC is seriously affected by the mismatch uncertainty. Kim *et al.* constructed a robust sliding hyperplane to deal with structural uncertainty using Riccati's inequality<sup>[36]</sup>. Choi *et al.* proposed a sliding surface design method based on linear matrix inequality (LMI) and guaranteed the existence of asymptotically stable sliding surfaces with full-order

sliding-mode dynamics<sup>[37]</sup>. Wen *et al.* proposed an adaptive sliding-mode control scheme<sup>[38]</sup>. The mismatch uncertainty considered by the above methods must be H2 paradigm bounded, which is an unreasonable assumption for practical systems. Utkin *et al.* proposed the integral SMC (I-SMC), which accumulates the error by an integral term so as to keep the error of the system zero even in the steady state, which can effectively suppress the effect of external perturbations on the system and reduce the jitter<sup>[39]</sup>. However, all of the above methods deal with the mismatch uncertainty by degrading the performance. Wei *et al.* incorporate the synergistic effect of SMC feedback and feedforward compensation based on disturbance estimation to construct a control law that improves the robustness and dynamic performance of the system<sup>[40]</sup>.

This study provides insights into exoskeleton control methods using a non-singular fast terminal sliding mode controller (NFTSMC) based on the nonlinear disturbance observer (NDO) framework. The main contributions of this manuscript are summarized below:

- (1) A trajectory planning method based on polynomial interpolation and optimization of the minimum jerk model has been proposed for exoskeleton rehabilitation robots. This method can generate a desired trajectory that conforms to the natural motion characteristics of the human body, achieving smooth and natural joint movements during rehabilitation training;
- (2) A motion-dependent switching function has been designed to achieve a smooth transition between normal training mode and safe stop mode. This function is crucial for protecting patient safety during rehabilitation training and avoiding discomfort or injury caused by sudden changes;
- (3) Non-singular fast terminal sliding mode (NFTSM) control based on NDO: A NFTSM control method based on a NDO has been proposed for precise tracking of the desired joint angles, with the aim of achieving a tracking error that tends to zero in a finite time. This method is robust against unknown bounded external disturbances and addresses the singularity and chattering issues associated with traditional SMC.

The rest of the paper is organized as follows: Section 2 describes the dynamic model of the upper limb rehabilitation robot. Section 3 describes the robot-assisted rehabilitation control strategy, and Section 4 validates the designed control algorithm through numerical simulation. Finally, Section 5 discusses and concludes this study.

## 2. PROBLEM FORMULATION

### 2.1. Notations, definitions, and lemmas

Notations:  $\mathbb{R}$ ,  $\mathbb{R}^n$ ,  $\mathbb{R}^{m \times n}$  represent the set of real numbers,  $n$  dimensional vectors space, and  $m \times n$  real matrices space, respectively. The maximum and minimum eigenvalues of the matrix  $\Phi \in \mathbb{R}^{m \times n}$  are defined by  $\lambda_{\max}(\Phi)$  and  $\lambda_{\min}(\Phi)$ , respectively. For  $\vartheta \in \mathbb{R}^n$ , denote  $\text{sig}^l(\vartheta) = \text{col}(\text{sig}^l(\vartheta_1), \dots, \text{sig}^l(\vartheta_n))$ ,  $\text{sig}^l(\vartheta_i) = \text{sgn}(\vartheta_i) |\vartheta_i|^l$  ( $i = 1, \dots, n$ ), and the signum function is given by

$$\text{sgn}(\vartheta_i) = \begin{cases} 1, & \vartheta_i > 0 \\ -1, & \vartheta_i < 0 \\ 0, & \vartheta_i = 0 \end{cases} \quad (1)$$

Lemma 1<sup>[41]</sup> Assume that there exists a continuous positive definite function  $V(t)$  which satisfies the following inequality:

$$\dot{V}(t) + \eta V(t) + \mu V^\nu(t) \leq 0 \quad (2)$$

Subsequently, the function  $V(t)$  approaches the equilibrium position within a finite time  $t_f$ :

$$t_f \leq \frac{1}{\eta(1+\nu)} \ln \frac{\eta V^{1-\nu}(t_0) + \mu}{\mu} \quad (3)$$

where  $\eta > 0$ ,  $\mu > 0$  and  $0 < \nu < 1$ .

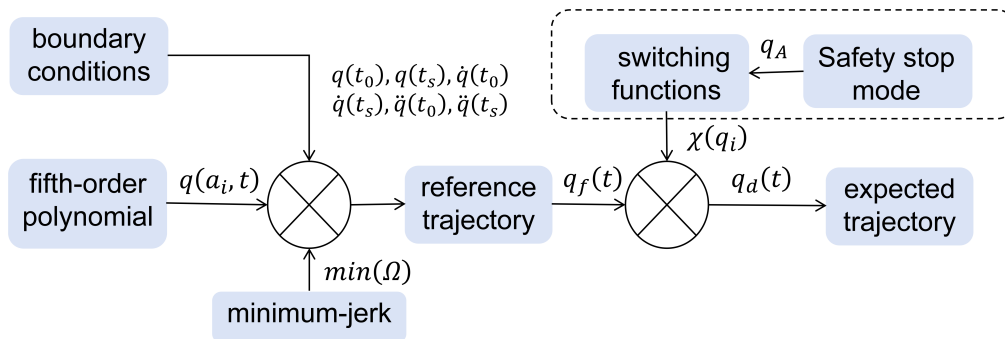


Figure 1. Trajectory planning structure diagram.

## 2.2. System modeling

Consider describing an exoskeleton system with systematic uncertainty and bounded disturbances in the following form:

$$M(q)\ddot{q} + C(q, \dot{q})\dot{q} + G(q) + \tau_d = \tau \quad (4)$$

where  $q = [q_1, \dots, q_n]^T$  denotes the angles of the five joints,  $\dot{q}$  and  $\ddot{q}$  represent joint velocity and acceleration, respectively,  $\tau = [\tau_1, \dots, \tau_n]^T \in \mathbb{R}^n$  denotes the input torque vector, and  $\tau_d = [\tau_{d1}, \dots, \tau_{dn}]^T \in \mathbb{R}^n$  represents the disturbance torque vector; the generalized inertia matrix  $M(q) \in \mathbb{R}^{n \times n}$ , corioles/centripetal matrix  $C(q, \dot{q}) \in \mathbb{R}^{n \times n}$  and gravity vector  $G(q) \in \mathbb{R}^{n \times 1}$ .

Due to the unavoidable uncertainty in the system, Equation (4) can be written as:

$$M_q\ddot{q} + C_q\dot{q} + G_q = \tau + M_qD \quad (5)$$

where

$$D = M_q^{-1}(-M_0(q)\ddot{q} - C_0(q, \dot{q})\dot{q} - G_0(q) - \tau_d)$$

with  $M_q = M(q) - M_0(q)$ ,  $C_q = C(q, \dot{q}) - C_0(q, \dot{q})$ ,  $G_q = G(q) - G_0(q)$ .  $M_q, C_q, G_q$  represent the values obtained from parameter identification<sup>[42]</sup> and  $M_0(q), C_0(q, \dot{q}), G_0(q)$  represent the system uncertainty, respectively.

Equation (5) can be further given as:

$$\ddot{q} = M_q^{-1}\tau - M_q^{-1}(C_q\dot{q} + G_q) + D \quad (6)$$

## 3. METHODS

### 3.1. Trajectory planning

Figure 1 illustrates the overall process of trajectory planning. In this paper, trajectory planning optimizes a constrained-time fifth-order polynomial using the minimum-jerk principle. The form of the fifth-order polynomial is:

$$q_i(t) = p_{oi} + p_{1i}t + p_{2i}t^2 + p_{3i}t^3 + p_{4i}t^4 + p_{5i}t^5 \quad (7)$$

where  $p_{oi}, \dots, p_{5i}$  are constants to be designed,  $i = 1, 2, \dots, n$ .

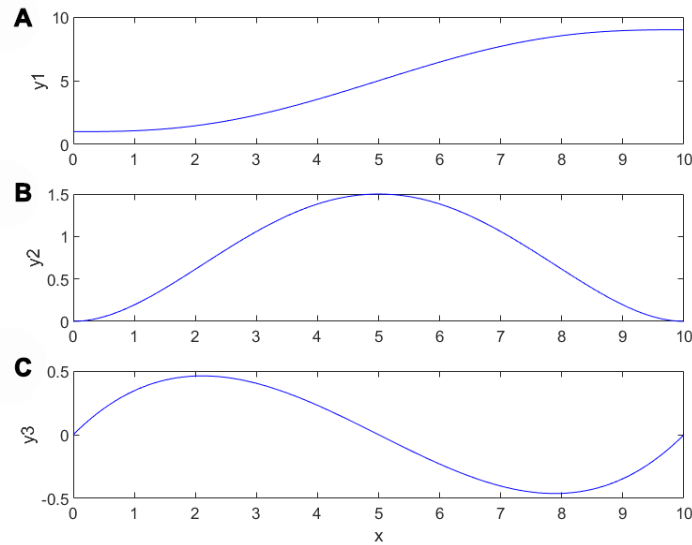


**Figure 2.** Reference trajectories and their first and second order derivative images in terms of  $t_z = 10$  and  $q_z = 8$ .

Sudden and abrupt movements can exacerbate mechanical wear and precipitate resonance in exoskeletons; hence, we aspire to ensure that the exoskeleton's trajectory is smooth. However, the specifics of certain motions are contingent upon their respective constraints. The spatial and temporal properties of the path are constrained by the position, velocity, and acceleration at the beginning (time = 0) and at the end (time = d) of the motion, as well as their maximum values. The selected constraints for point-to-point motion are as follows:

$$\left\{ \begin{array}{l} q(t_o) = q_o \\ q(t_s) = q_s \\ \dot{q}(t_o) = 0 \\ \dot{q}(t_s) = 0 \\ \ddot{q}(t_o) = 0 \\ \ddot{q}(t_s) = 0 \\ \|q(t)\|_{\infty} \leq q_m \\ \|\dot{q}(t)\|_{\infty} \leq \dot{q}_m \\ \|\ddot{q}(t)\|_{\infty} \leq \ddot{q}_m \end{array} \right. \quad (8)$$

where  $t_o$  is the starting moment and  $t_s$  is the ending moment,  $q_o$ ,  $q_s$  are the joint angles at the initial and end positions respectively,  $q_m$ ,  $\dot{q}_m$ , and  $\ddot{q}_m$  are the maximum values of position, velocity and acceleration, respectively.

The objective is to achieve the maximum degree of smoothness, which is accomplished by minimizing the mean-square jerk. Jerk, by its mathematical definition, is the derivative of acceleration. Consequently, the minimum-jerk model can be expressed as

$$\Omega = \frac{1}{2} \int_{t_o}^{t_s} (j_i) dt \quad (9)$$

where  $j_i = \frac{d^3 q_i(t)}{dt^3}$  denotes jerk.

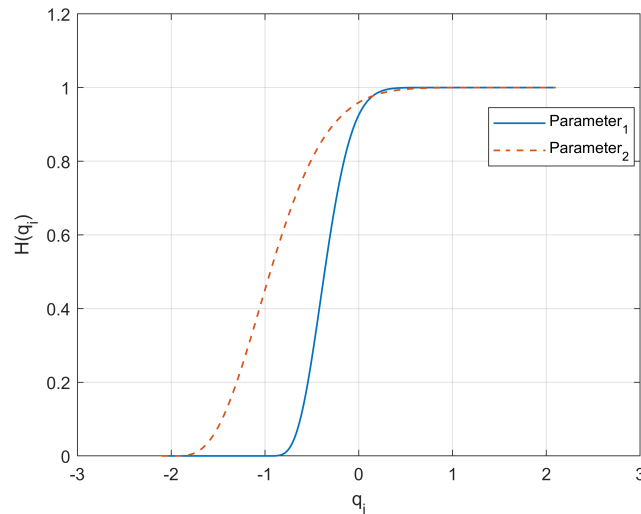


**Figure 3.** H-function images with different parameters.

Combining Equation (8), solving for the constant  $p_0, \dots, p_5$  yields<sup>[43]</sup>:

$$q_r = q_b + q_z \left[ 10 \left( \frac{t}{t_z} \right)^3 - 15 \left( \frac{t}{t_z} \right)^4 + 6 \left( \frac{t}{t_z} \right)^5 \right] \quad (10)$$

where  $t_z = t_o - t_s$  represents the duration, and  $q_z = q_o - q_s$  represents the amplitude of motion.

Modifications to the  $t_z$  or  $q_z$  are employed solely for the purpose of altering the scale of the position and time axes, respectively. The image of the trajectory with  $t_z = 10$  and  $q_z = 8$  is shown in Figure 2, where  $y_2$  is the first order derivative of  $y_1$  and  $y_3$  is the second order derivative of  $y_1$ , and the following properties can be defined:

$$\begin{aligned} \dot{q}_m &= 1.88 \frac{q_z}{t_z} \\ \ddot{q}_m &= 5.77 \frac{q_z}{t_z^2} \end{aligned} \quad (11)$$

In order to enhance the safety of the entire robotic system, this paper establishes a safety stop mode. When the end-effector is detected within the safety stop area, the robot will gradually cease its training movements and return to the designated safe position to prevent any potential harm. To achieve a smooth transition between normal training and safety stopping, the following motion-related transition functions<sup>[30]</sup> are employed to provide a buffer zone.

$$H(q_{i,j}) = \begin{cases} 0, & q_{i,j} \leq c_1 \\ b_1 \left( \left( \frac{q_{i,j} - c_1}{c_2 - c_1} - 1 \right)^4 - 1 \right)^{a_1} \\ + b_2 \left( \left( \frac{q_{i,j} - c_1}{c_2 - c_1} - 1 \right)^4 - 1 \right)^{a_2}, & c_1 < q_{i,j} < c_2 \\ 1, & q_{i,j} \geq c_2 \end{cases} \quad (12)$$

where  $q_{i,j}$  denotes the value of  $q_i$  at the  $j$ th sampling,  $a_2 = a_1 + 2$ ,  $b_1 = \frac{a_2}{2}$ ,  $b_2 = -b_1 + 1$  denote the constants that satisfy the conditions and in order to guarantee the desired trajectory is at least twice differentiable, it is necessary that  $a_1 > 4$  is an even number.  $c_1$  and  $c_2$  denote the boundaries of the buffer region, respectively.

Equation (12) provides a buffer smoothing transition between  $c_1$  and  $c_2$  by a combination of two power functions. The smoothness and shape of the transition can be controlled by adjusting the values of the parameters.

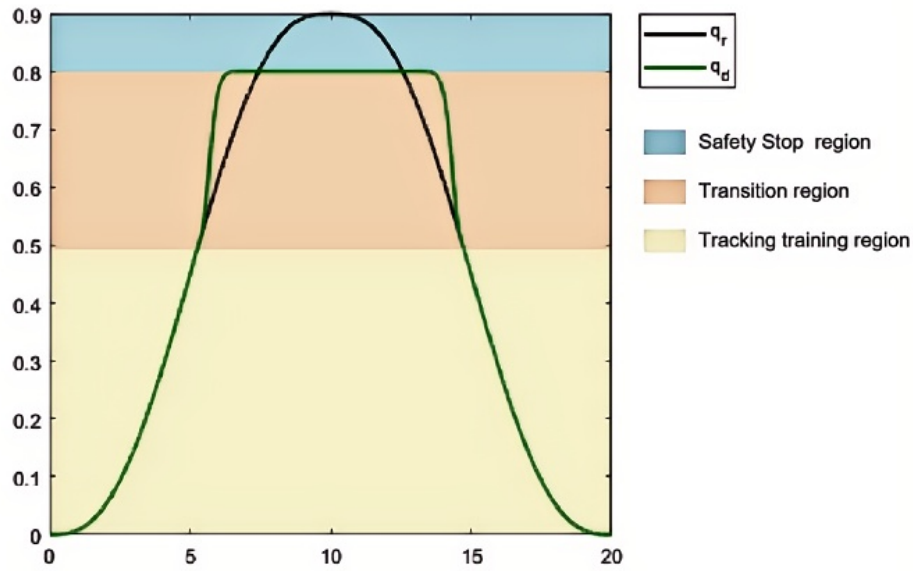


Figure 4. Schematic of the desired trajectory under the motion switching function.

As shown in Figure 3, where  $\text{Params}_i = [c_1 \ c_2 \ b_1 \ b_2 \ a_1 \ a_2]$ ,  $\text{Params}_1 = [-1 \ 1 \ 4 \ -3 \ 6 \ 8]$  and  $\text{Params}_2 = [-2 \ 2 \ 3 \ -2 \ 4 \ 6]$ , a larger value of the exponent will make the transition steeper, while a smaller value of the exponent will make the transition smoother. This function can be utilized to regulate the robot's behavior, for instance, enabling a gradual transition from safe stop mode to normal operation mode.

Therefore, the desired trajectory is designed as:

$$q_{di} = H(q_{i,j}) q_{ri} + (1 - H(q_{i,j})) q_{Ai} \quad (13)$$

where  $q_A = [q_{A1}, \dots, q_{An}]^T$  is stop position in safety stop mode.

Using the physical properties of the switching function, we can divide the workspace into three regions: the tracking training region, the transition region and the safe stopping region, as shown in Figure 4. When the desired trajectory  $q_d$  is smaller than the boundary of the transition region  $c_1$ , it is consistent with the reference trajectory  $q_r$ ; when the reference trajectory is in the transition region, the switching function  $H$  is responsible for realizing the smooth transition from the tracking training region to the safe stopping region; and when the reference trajectory is larger than the boundary of the transition region, the desired trajectory will stay at a safe position to ensure the safety of the subject.

### 3.2. NDO design

The disturbance signals considered in this paper are the input torque of the human and system uncertainty body and unknown external vibrations. Assume that  $\hat{D}$  is the estimate of the disturbance  $D$ . The nonlinear perturbation observer is designed as follows

$$\begin{aligned} \hat{D} &= -K_1 w - K_2 \text{sig}^t(w) - K_3 \text{sgn}(w) \\ w &= z - \dot{q} \\ \dot{z} &= -K_1 w - K_2 \text{sig}^t(w) - K_3 \text{sgn}(w) - M_q^{-1} (C_q \dot{q} + G_q) + M_q^{-1} \tau \end{aligned} \quad (14)$$

where  $w$  is a defined auxiliary variable for the convenience of NDO design and  $K_1, K_2$  are the gain matrixes to be designed,  $K_1 = \text{diag} \{k_{11}, \dots, k_{1n}\}$ ,  $K_2 = \text{diag} \{k_{21}, \dots, k_{2n}\}$ ,  $K_3 = \text{diag} \{k_{31}, \dots, k_{3n}\}$  and  $0 < \iota < 1$ .

**Theorem 1:** In consideration of the exoskeleton system Equation (5), the DOC is designed in accordance with Equation (14). Subsequently, the disturbance approximation error of the proposed DOC is shown to be convergent in a finite time.

**Proof:** Let us define  $\tilde{D} = \hat{D} - D$ . Then, from Equations (5) and (14) it follows that:

$$\begin{aligned}\tilde{D} &= -K_1 w - K_2 \text{sig}^\iota(w) - K_3 \text{sgn}(w) - \ddot{q} - M_q^{-1}(C_q \dot{q} + G_q) + M_q^{-1} \tau \\ &= \dot{z} - \ddot{q} \\ &= \dot{w}\end{aligned}\quad (15)$$

Therefore, it can be concluded that the convergence of the disturbance error is consistent with the convergence of the auxiliary variables  $s_1$ . Choose the Lyapunov function candidate as:

$$V_1 = \frac{1}{2} w^T w \quad (16)$$

The time derivative of  $V_1$  is given by

$$\begin{aligned}\dot{V}_1 &= w^T \dot{w} \\ &= w^T (\dot{z} - \ddot{q}) \\ &= w^T \left( \dot{z} + M_q^{-1}(C_q \dot{q} + G_q) - M_q^{-1} \tau - D \right) \\ &= w^T (-K_1 w - K_2 \text{sig}^\iota(w) - K_3 \text{sgn}(w) - D) \\ &\leq -w^T K_1 w - w^T K_2 \text{sig}^\iota(w) - K_3 \|w\| + \|w\| \|D\| \\ &\leq -w^T K_1 w - w^T K_2 \text{sig}^\iota(w) \\ &\leq -2k_1 V_1 - 2^{\frac{\iota+1}{2}} k_2 V_1^{\frac{\iota+1}{2}}\end{aligned}\quad (17)$$

where  $k_1 = \lambda_{\min}(K_1)$  and  $k_2 = \lambda_{\min}(K_2), k_3 = \lambda_{\min}(K_3)$  and  $k_3 \geq \|D\|$ .

According to Lemma 1, the auxiliary variable  $s_1$  converges to the equilibrium point in the finite time  $t_1$  defined by

$$t_1 \leq \frac{1}{k_1(1-\iota)} \ln \frac{2k_1 V^{\frac{1-\iota}{2}} + 2^{\frac{\iota+1}{2}} k_2}{2^{\frac{\iota+1}{2}} k_2} \quad (18)$$

In light of the finite time convergence property of the auxiliary variable  $s_1$ , it can be concluded that the disturbance approximation error of the proposed disturbance observer is convergent in a finite time.

### 3.3. NFTSMC design

Furthermore, a NFTSM control method based on NDO is proposed as a means of enhancing the performance of the control system. In the NFTSMC design, the singular value problem is circumvented and rapid convergence is attained through a modified terminal sliding mode surface. The overview of the NFTSMC framework is illustrated in Figure 5, which provides a detailed view of the structure and key components of the control strategy.

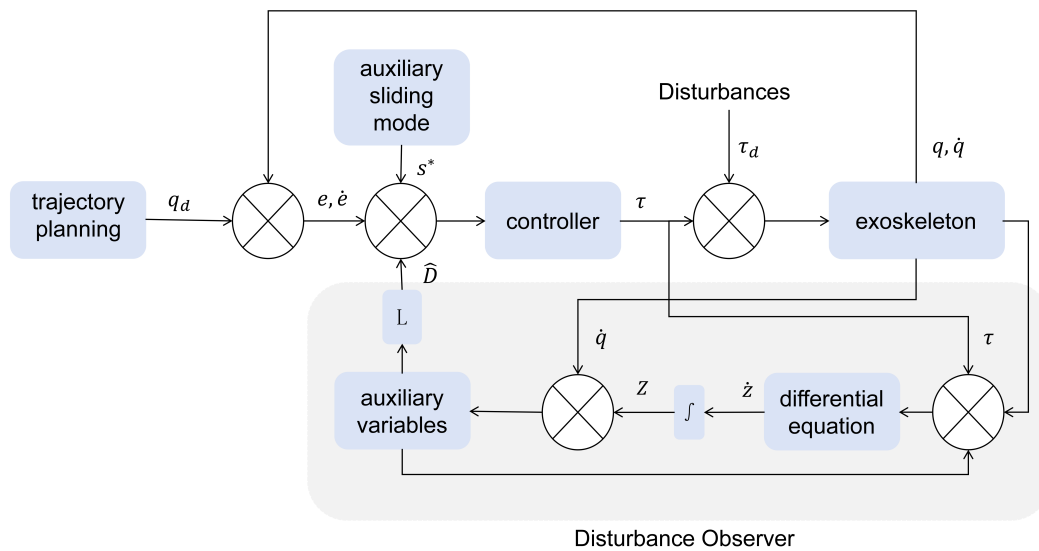


**Figure 5.** Overview of the NFTSMC framework. NFTSMC: Non-singular fast terminal sliding mode controller.

The tracking error is defined as follows:

$$e = q_d - q \quad (19)$$

To circumvent the issue of singular values, an improved terminal sliding surface<sup>[44]</sup> is designed as:

$$s = \dot{e} + L_1 \Psi(e) + L_2 e \quad (20)$$

where

$$\Psi(e) = \begin{cases} \text{sig}^\gamma(e), s^* = 0 / s^* \neq 0, |e| \geq \mu \\ x_1 e + x_2 \text{sig}^2(e), s^* \neq 0, |e| < \mu \end{cases}$$

with  $s^* = \dot{e} + L_1 \text{sig}^\gamma(e)$ ,  $L_1 = \text{diag}(l_{11}, \dots, l_{1n})$ ,  $L_2 = \text{diag}(l_{21}, \dots, l_{2n})$ ,  $\gamma \in (0.5, 1)$ ,  $\mu > 0$ ,  $x_1 = (2 - \gamma) \mu^{\gamma-1}$ ,  $x_2 = (\gamma - 1) \mu^{\gamma-2}$ .

The nonlinear term  $\Psi(e)$  plays a crucial role in the design of the sliding mode surface, providing the system with additional control authority and robustness. Specifically, the desired value of the sliding mode surface  $s$  is denoted by  $s^*$ , where  $s^* = 0$  represents the system being in equilibrium, while  $s^* \neq 0$  indicates that the system is in a non-equilibrium state. When the system is in equilibrium, it means that the system has reached the desired equilibrium point but still needs to remain at that point. At this stage, the objective of SMC is to ensure stability near the equilibrium point and to resist external disturbances or parameter variations. The control signal in the form of  $\text{sig}^\gamma(e)$  can quickly correct minor deviations from the equilibrium point. When the system is in a high error state, the absolute value of the error  $e$  exceeds a predefined threshold  $\mu$ . In this case, the system needs to rapidly reduce the error to approach the desired value as soon as possible. The control signal in the form of  $\text{sig}^\gamma(e)$  provides sufficient control authority to ensure rapid convergence when the error is large.

When the error  $e$  is small, the system requires more precise control to avoid excessive adjustments that may lead to chattering or instability. At this stage, the nonlinear term  $\Psi(e)$  takes the form of a combination of linear

and nonlinear components. The linear term  $x_1 e$  provides stable feedback control, which helps maintain system stability, while the nonlinear term  $x_2 \text{sig}^2$  offers additional control authority when the error approaches zero, ensuring that the system can accurately reach the desired value. The design of the nonlinear term  $\Psi(e)$  takes into account the system's rapid convergence, stability, and robustness. Using the same nonlinear control form  $\text{sig}^\gamma(e)$  in both equilibrium and large error phases simplifies the control strategy design while ensuring that the system can provide effective control signals in different stages. This design effectively reduces the system's convergence time and prevents oscillations or instability near the equilibrium point.

Differentiating Equation (20), and considering Equation (6) yield:

$$\begin{aligned}\dot{s} &= \ddot{e} + L_1 \dot{\Psi}(e) + L_2 \dot{e} \\ &= \ddot{q}_d - \ddot{q} + L_1 \dot{\Psi}(e) + L_2 \dot{e} \\ &= \ddot{q}_d + M_q^{-1} (C_q \dot{q} + G_q) - M_q^{-1} \tau - D + L_1 \dot{\Psi}(e) + L_2 \dot{e}\end{aligned}\quad (21)$$

where

$$\dot{\Psi}(e) = \begin{cases} \gamma |e|^{\gamma-1} \dot{e}, s^* = 0/s^* \neq 0, |e| \geq \mu \\ x_1 \dot{e} + 2x_2 |e| \dot{e}, s^* \neq 0, |e| < \mu \end{cases}$$

The NDO-based NFSMC controller is then given by:

$$\tau = M_q \ddot{q}_d + C_q \dot{q} + G_q - M_q \hat{D} + M_q (L_3 \text{sig}^\alpha(s) + L_4 s - L_5 \text{sgn}(s) + L_1 \dot{\Psi}(e) + L_2 \dot{e}) \quad (22)$$

where  $L_3 = \text{diag}(l_{31}, \dots, l_{3n})$ ,  $L_4 = \text{diag}(l_{41}, \dots, l_{4n})$ ,  $L_5 = \text{diag}(l_{51}, \dots, l_{5n})$ ,  $\alpha \in (0, 1)$ .

Considering the uncertain nonlinear system represented by Equation (5), which is subject to an external disturbance, a terminal sliding mode disturbance observer is designed in Equation (14). Under the NFTSMC is constructed as Equation (22), all signals of the closed-loop system are shown to converge in a finite time.

Choose the Lyapunov function  $V$  as:

$$V_2 = \frac{1}{2} s^T s \quad (23)$$

Substituting Equation (22) into the derivative of the Lyapunov function, we obtain:

$$\begin{aligned}\dot{V}_2 &= s^T \dot{s} \\ &= s^T \left( \ddot{q}_d + M_q^{-1} (C_q \dot{q} + G_q) - M_q^{-1} \tau - D + L_1 \dot{\Psi}(e) + L_2 \dot{e} \right) \\ &= s^T (-L_3 \text{sig}^\alpha(s) - L_4 s - L_5 \text{sgn}(s) + \hat{D} - D) \\ &= s^T (-L_3 \text{sig}^\alpha(s) - L_4 s - L_5 \text{sgn}(s) + \tilde{D}) \\ &\leq s^T (-L_3 \text{sig}^\alpha(s) - L_4 s) - L_5 \|s\| + \|s\| \|\tilde{D}\| \\ &\leq -s^T L_3 \text{sig}^\alpha(s) - s^T L_4 s \\ &\leq -l_3 \|s\|^{\frac{\alpha+1}{2}} - l_4 \|s\|^2\end{aligned}\quad (24)$$

where  $l_3 = \lambda_{\min}(L_3)$  and  $l_4 = \lambda_{\min}(L_4)$ ,  $l_5 = \lambda_{\min}(L_5)$  and  $l_5 \geq \|\tilde{D}\|$ .

Invoking Equations (23) and (24) are written as:

$$\dot{V}_2 \leq -2^{\frac{\alpha+1}{2}} l_3 V_2^{\frac{\alpha+1}{2}} - 2l_4 V_2 \quad (25)$$

Based on Equation (25), we can conclude that the system is stable and the state of the system will converge to the stable point as the  $V_2$  decreases. The value of  $l_3$  and  $l_4$  has a significant effect on the rate of convergence,

while the value of  $\alpha$  affects the contribution of the nonlinear term to the rate of convergence. Furthermore, from Lemma 1, it can be concluded that the system's tracking error can be driven to  $s = 0$  within finite time.

$$t \leq \frac{1}{l_4(1-\alpha)} \ln \frac{2l_4V^{\frac{1-\alpha}{2}} + 2^{\frac{\alpha+1}{2}}l_3}{2^{\frac{\alpha+1}{2}}l_3} \quad (26)$$

Next, Equation (22) is substituted into Equation (6) to derive the sliding motion equations. Subsequently, a stability analysis of the sliding motion is conducted. Given the considerations of  $\dot{e} = 0$  and  $\ddot{D} = 0$ , the following can be derived:

$$\ddot{e} = -l_3 \text{sig}^\alpha(s) - l_4 s + l_5 \text{sgn}(s) \quad (27)$$

In finite-time control, the objective is to ensure that the error converges to zero within a finite time interval, rather than merely driving the derivative of the error to zero. Therefore,  $\dot{e} = 0$  itself is not an attractor. Instead, the control law is designed such that both the error  $e$  and its derivative  $\dot{e}$  converge to zero in finite time<sup>[46]</sup>.

## 4. SIMULATION

The simulation is distributed into two parts: one is the trajectory planning based on the motion switching function, and the other part is the control method for tracking the generated trajectory. The control method simulation uses two passive rehabilitation training control methods: one based on a linear SMC algorithm and the other based on a non-singular TSMC algorithm with a perturbation observer. The joint tracking error data were recorded during the training process.

In order to verify the performance of the proposed control framework, a series of simulation experiments are conducted using MATLAB. A point-to-point arrival task is selected for the experiment, where task points  $q_1 = [0 \quad -0.1 \quad -0.3 \quad 0.6 \quad -0.7]^T$  and the farthest position  $q_2 = [0.9 \quad 4 \quad 5.5 \quad 5.5 \quad 5]^T$ .

### 4.1. System modeling

In this paper, the simulation uses a 5 degrees of freedom (5-DOF) upper-limb exoskeleton model<sup>[45]</sup>. The schematic diagram of the exoskeleton robot is shown in Figure 6, which illustrates the structure and key components of the device. The robot dynamics can be referred to Equation (4). The details are as follows:

$$M(q) = \begin{bmatrix} M_{11} & M_{12} & M_{13} & 0 & 0 \\ M_{21} & M_{22} & M_{23} & 0 & 0 \\ M_{31} & M_{32} & M_{33} & 0 & M_{35} \\ 0 & 0 & 0 & M_{44} & 0 \\ 0 & 0 & M_{53} & 0 & M_{55} \end{bmatrix}$$

$$C(q, \dot{q}) = \begin{bmatrix} C_1\dot{q}_2 & C_2\dot{q}_3 + C_3\dot{q}_2 & C_4\dot{q}_2 + C_5\dot{q}_3 & 0 & 0 \\ C_6\dot{q}_1 & C_7\dot{q}_3 & C_8\dot{q}_3 & 0 & 0 \\ C_5\dot{q}_1 & C_9\dot{q}_2 & 0 & 0 & 0 \\ C_{10}\dot{q}_2 & 0 & C_{11}\dot{q}_2 & 0 & 0 \\ 0 & C_{12}\dot{q}_2 & 0 & 0 & 0 \end{bmatrix}$$

$$G(q) = [0 \quad G_2 \quad G_3 \quad 0 \quad G_5]^T$$

### 4.2. Trajectory planning

Consider a fifth-order polynomial for trajectory planning based on the optimization of the minimum-jerk principle, where the initial position  $q_1$  and the farthest position  $q_2$ . The motion trajectory path is a reciprocal motion first from  $q_1$  to  $q_2$  and then back to  $q_1$  as shown in Figure 7. It should be noted that the reference

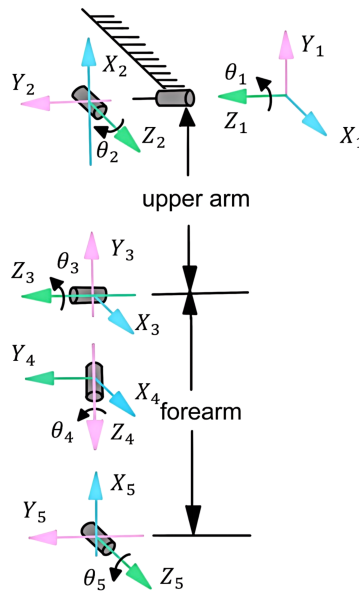


**Figure 6.** Schematic diagram of a 5-DOF upper-limb exoskeleton robot. 5-DOF: 5 Degrees of freedom.

joint angle is depicted as a constant value at the end of the movement. This is because the figure illustrates the trajectory planning between two specific target points for simplicity. In practice, the overall trajectory is decomposed into multiple smaller segments, each planned using fifth-order polynomial interpolation. By connecting these segments sequentially, a continuous and smooth trajectory is formed, allowing the exoskeleton to perform complex and dynamic tasks rather than maintaining a single position.

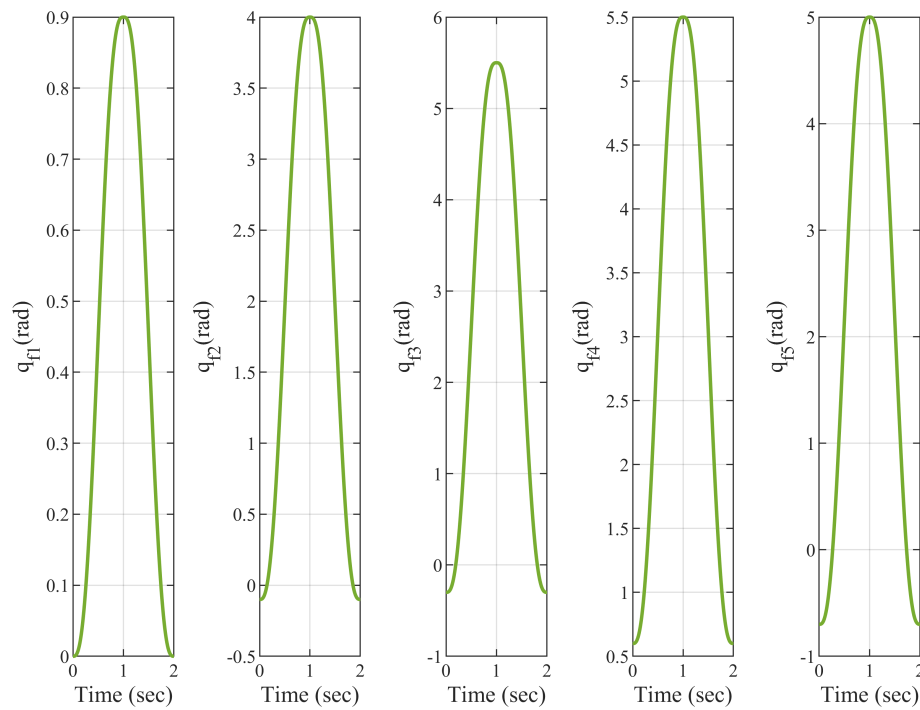
If the safe position is artificially set to  $q_A = [0.9 \ 4 \ 5.5 \ 5.5 \ 5]^T$ , the region beyond this position is set as the safe stopping region. According to Equation (13), the desired trajectory  $q_d$  adjusted by the switching function is shown in Figure 8. In which, the parameters in Equation (12) are set to  $a_1 = 4$ ,  $a_2 = 6$ ,  $b_1 = 3$ ,  $b_2 = -2$ .

Figure 8 shows that when the reference trajectory is close to the safe position, the desired trajectory enters the transition region and switches to the safe position under the action of the switching function, and when the reference trajectory has entered the safe stopping region, the desired trajectory stays in the safe stopping position until the reference trajectory leaves the safe stopping region, and then once again smoothly switches to the tracking training mode.

Then, the sliding variable can be easily calculated based on the tracking error between the desired trajectory and the actual trajectory. Thus, the robot can achieve perfect tracking by reducing the sliding film error.

#### 4.3. NFTSMC controller simulation

In order to underscore the enhanced efficacy of the proposed NFTSMC scheme in realizing faster and higher precision tracking, this study engages in a comparative analysis with two additional control methodologies. The control strategies selected for this comparative investigation are TSMC [46] and non-singular TSMC (NTSMC) [47]. The comparative experiments within this paper will assess the performance of the NFTSMC scheme against the TSMC and NTSMC approaches across a spectrum of criteria, encompassing convergence velocity, tracking accuracy, robustness to parameter variations, and the stability of output torque. It is anticipated that the outcomes will accentuate the superior performance of the NFTSMC scheme in delivering expedited and



**Figure 7.** Trajectories based on minimum-jerk optimization.

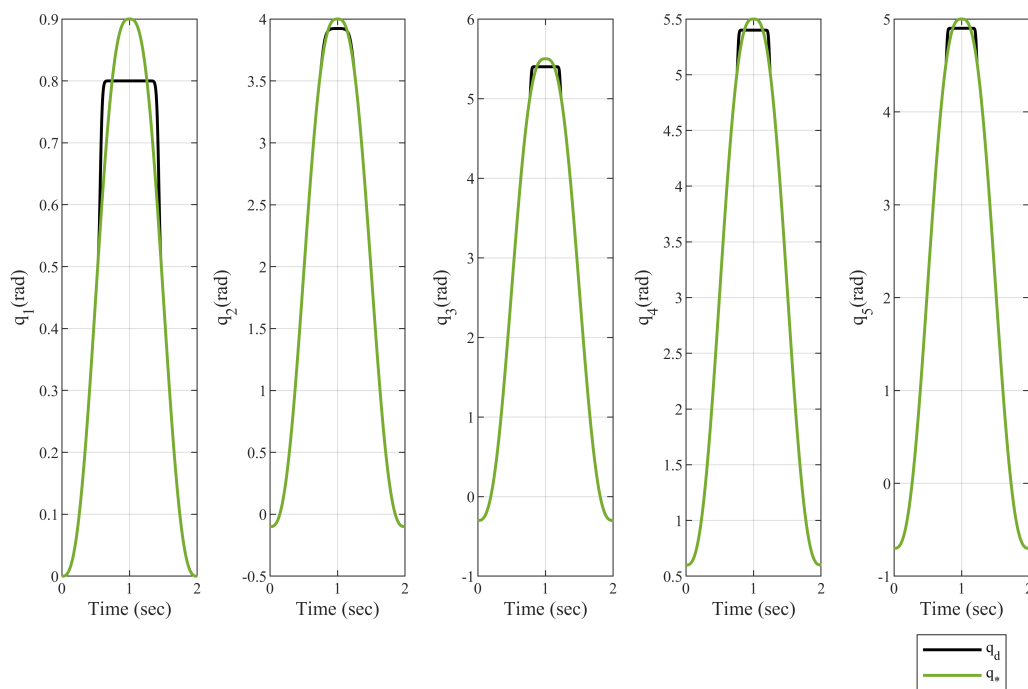


**Figure 8.** Desired trajectory with safe switching.

more precise tracking capabilities in contrast to the conventional TSMC and NTSMC methods. It is worth noting that the human force exerted by the patient on the exoskeleton under the passive training effect is

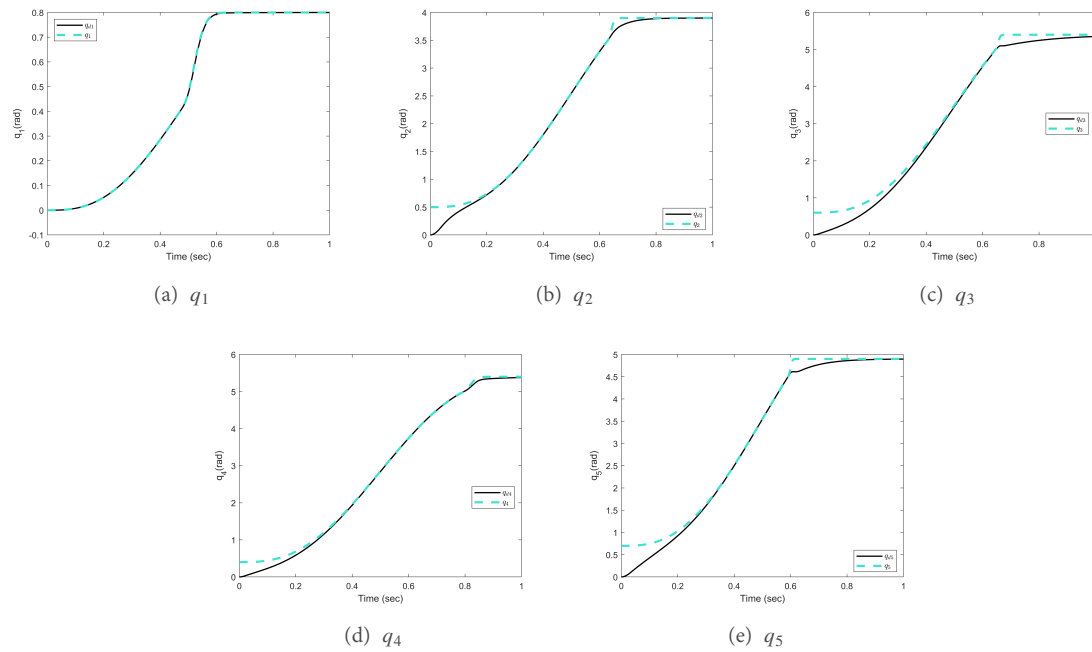


**Figure 9.** Output tracking in the case of NFTSMC. NFTSMC: Non-singular fast terminal sliding mode controller.

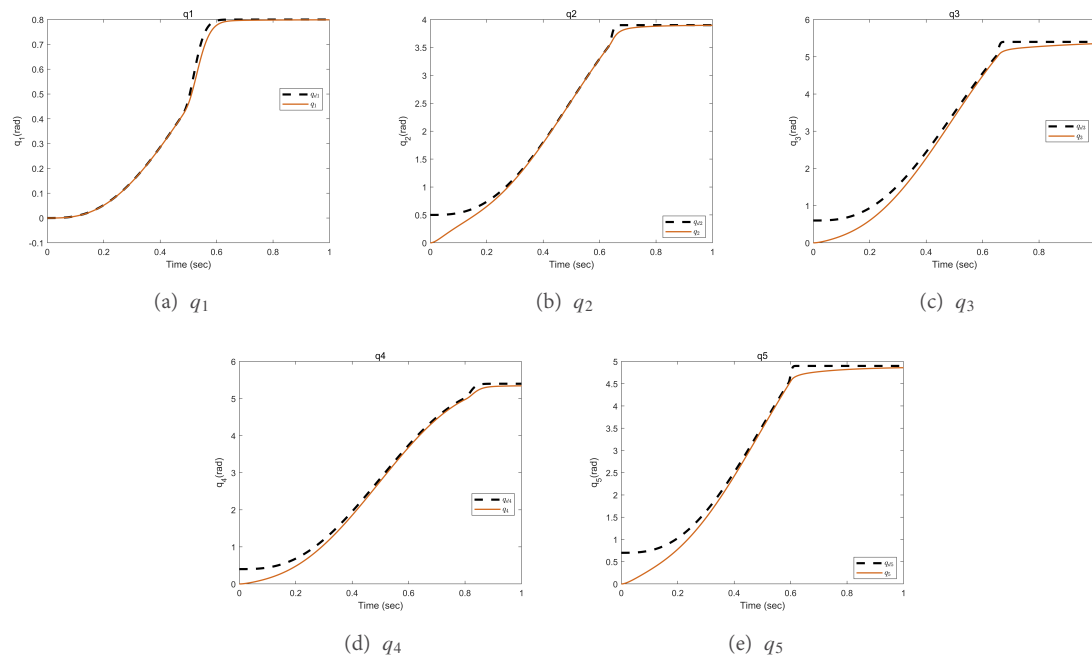


**Figure 10.** Output tracking in the case of TSMC. TSMC: Terminal sliding mode control.

regarded as the interference force. In consideration of the periodic interference effect that occurs in the actual training, the interference force is set as in this paper:  $\tau_{d1} = 1 + 0.5 \sin(t + \frac{\pi}{6})$ ,  $\tau_{d2} = 2 + 0.5 \sin(t - \frac{\pi}{6})$ ,  $\tau_{d3} = 2 + 0.5 \cos(t - \frac{\pi}{6})$ ,  $\tau_{d4} = 1 + 0.8 \sin(t - \frac{\pi}{6})$ ,  $\tau_{d5} = 1 + 0.5 \sin(t - \frac{\pi}{6})$ . The disturbance observer parameters and controller parameters are given as  $K_1 = \text{diag} [ 5 \ 10 \ 3 \ 4 \ 6 ]$ ,  $K_2 = \text{diag} [ 10 \ 20 \ 20 \ 20 \ 20 ]$ ,  $L_1 = \text{diag} [ 5 \ 6 \ 3 \ 5 \ 6 ]$ ,  $L_2 = \text{diag} [ 50 \ 50 \ 50 \ 50 \ 50 ]$ ,  $L_3 = \text{diag} [ 3 \ 4 \ 5 \ 4 \ 6 ]$ ,  $L_4 =$

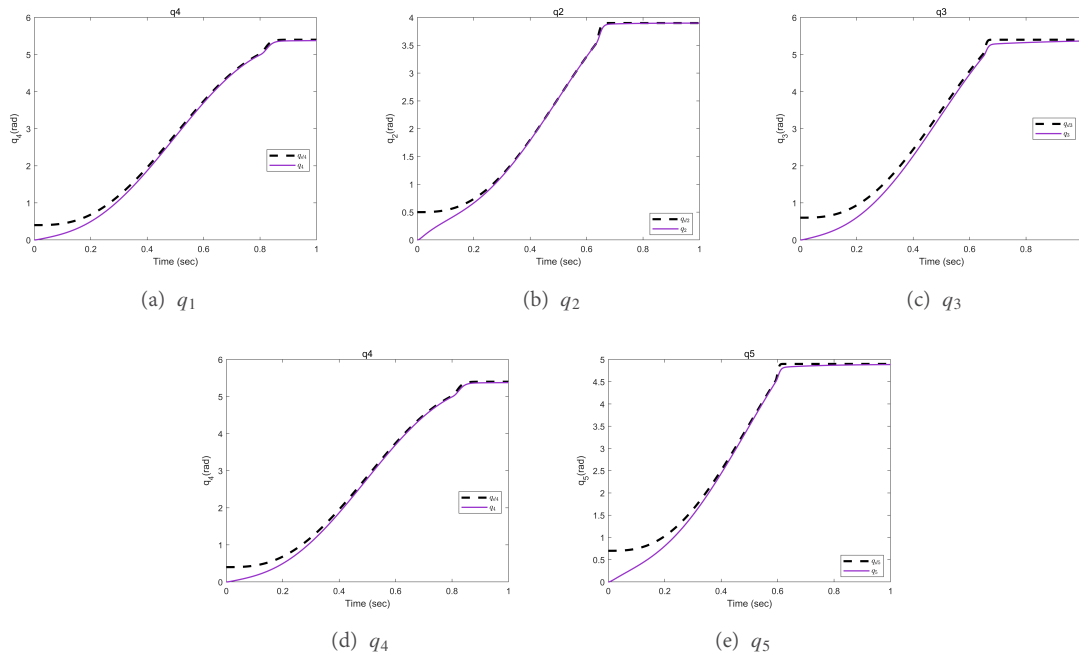


**Figure 11.** Output tracking in the case of NTSMC. NTSMC: Non-singular terminal sliding mode control.

$\text{diag} [ 40 \ 40 \ 40 \ 40 \ 40 ], \iota = 0.5, \gamma = 0.55, \alpha = 0.6.$

Based on the control parameters previously determined, the numerical simulation results of the controller have been obtained and are presented in Figures 9-11, respectively. This figure comprehensively demonstrates the performance of the controller by comparing the desired trajectory with the actual output trajectory. We consider tracking the same segment (from  $q_1$  to  $q_2$ ) of the desired trajectory as a representative example.

In Figure 9, the black curve represents the desired trajectory, which is the path that the system is expected to follow. On the other hand, the blue dashed line represents the actual output trajectory, which is the path that the system follows under the control of the proposed NFTSMC method. The simulation results shown in Figure 9 indicate that the NFTSMC method effectively tracks the desired trajectory. The close alignment between the black curve and the blue dashed line demonstrates that the system's output closely matches the desired path. This alignment confirms the effectiveness of the NFTSMC method in guiding the system toward the desired trajectory with high precision.

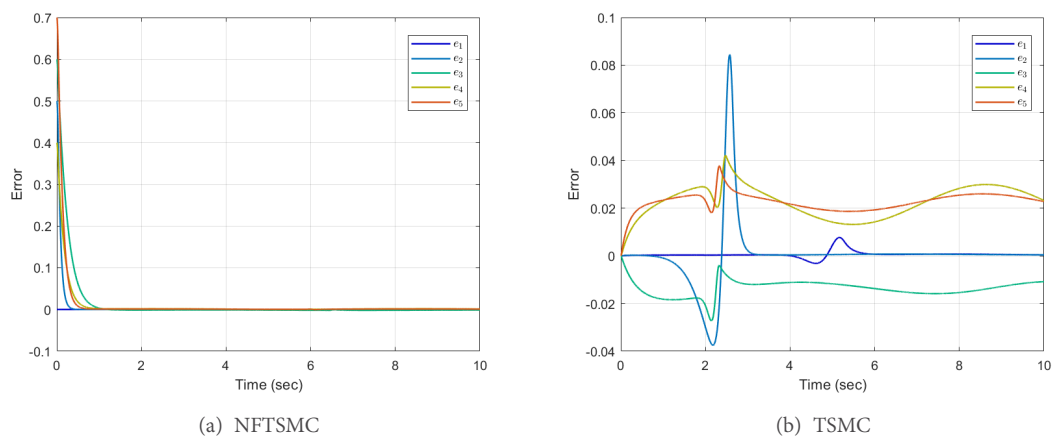
Figure 10 presents the tracking results for the TSMC method. This figure allows for an assessment of the tracking capabilities of TSMC, including its response to disturbances and its ability to maintain stability. The plot may reveal some deviations from the desired trajectory, indicating areas where TSMC may not be as effective as NFTSMC, particularly in terms of tracking accuracy and robustness against perturbations.

Figure 11 displays the tracking outcomes for the NTSMC method. This figure is crucial for evaluating NTSMC's performance in tracking the desired trajectory, especially in terms of its terminal phase behavior and its ability to achieve fast convergence. The plot may exhibit characteristics such as chattering, which is a common issue in traditional SMCs, and may affect the smoothness of the tracking trajectory. To quantify and compare the performance of these controllers, we calculated the root mean square (RMS) and mean absolute error (MAE) and summarized the results in Table 1. NFSMC exhibited the best performance in terms of both RMS and MAE, indicating higher precision and stability in joint angle control.

**Table 1. Controller error metrics: RMS and MAE**

Controller type	NFTSMC	NTSMC	TSMC
RMS(°)	0.5020	0.5600	0.6020
MAE(°)	0.4400	0.4550	0.6600

RMS: Root mean square; MAE: mean absolute error; NFTSMC: non-singular fast terminal sliding mode controller; NTSMC: non-singular terminal sliding mode control; TSMC: terminal sliding mode control.



**Figure 12.** Tracking error in the case of NFTSMC and TSMC. NFTSMC: non-singular fast terminal sliding mode controller; TSMC: terminal sliding mode control.

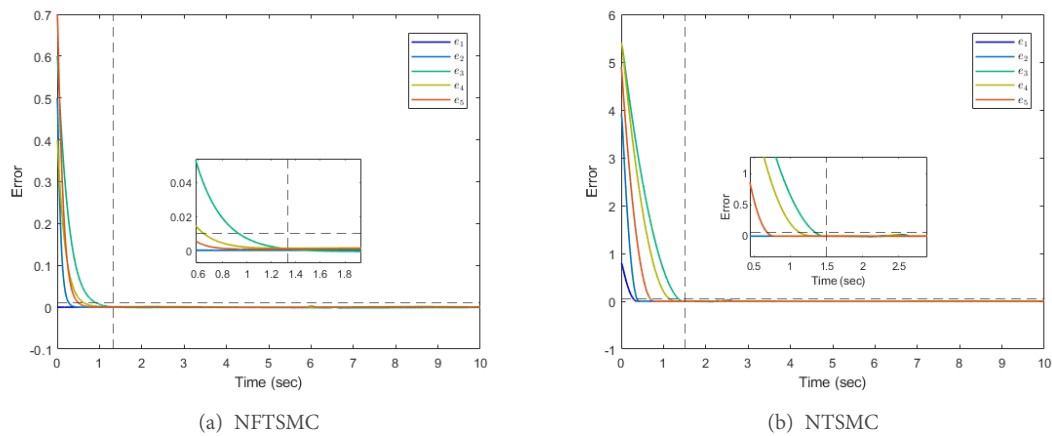


**Figure 13.** Tracking error in the case of NFTSMC and NTSMC. NFTSMC: Non-singular fast terminal sliding mode controller; NTSMC: non-singular terminal sliding mode control.

The tracking performance comparison between the NFTSMC and the TSMC, as shown in Figure 12, is presented with the error extended over a longer time span to facilitate a clearer observation of the differences. As depicted in the figure, the tracking error plot for NFTSMC [Figure 12A] exhibits a clear trend towards convergence, ultimately stabilizing at a negligible value. This indicates that the system's output, under the control

of NFTSMC, closely follows the desired reference trajectory with minimal deviation. In contrast, the TSMC tracking error plot [Figure 12B], while consistently maintaining a smaller value than NFTSMC, is characterized by a continuous fluctuating process. These fluctuations suggest that TSMC, despite having smaller error values, is unable to achieve the same level of stability and precision as NFTSMC. The sustained oscillations in the TSMC error curve prevent it from converging to a smaller value. Furthermore, the capacity of NFTSMC to maintain a low tracking error even when faced with parameter changes or external perturbations demonstrates its enhanced robustness.

In summary, the comparative analysis of the tracking error plots reveals that NFTSMC not only achieves higher tracking accuracy by bringing the system output closer to the desired trajectory but also exhibits better stability and robustness compared to TSMC. These attributes make NFTSMC a more reliable choice for applications where precise and stable tracking is paramount.

As can be seen from Figure 13, in the experimental analysis comparing the NFTSMC and NTSMC control strategies, the system error is intentionally extended over a longer time span to facilitate clearer observation. It is observed that both methods are capable of steering the system error towards a vicinity of zero within a relatively brief timeframe. However, an examination of the error curves reveals that the NFTSMC exhibits a more rapid convergence, signifying its superior response time. Additionally, NTSMC encounters specific data constraints during experimentation, which may impair its performance in real-world applications. The NTSMC is prone to singular value issues when managing data, which can result in the instability or diminished efficacy of the control algorithm. NFTSMC circumvents these challenges by employing a non-singular sliding surface design, which bolsters the system's robustness and stability. This design accounts for the dynamic properties and potential perturbations of the system, ensuring the control strategy's efficacy amidst uncertainties and external disturbances. Furthermore, NFTSMC incorporates a rapidly converging sliding surface and an innovative control law, which not only enhances the system's response velocity but also mitigates the occurrence of chattering phenomena.

Figures 14 and 15 show the performance of NFTSMC and NTSMC in terms of torque output, respectively. The torque diagram of NFTSMC shows smoother torque variation than that of NTSMC, which indicates that NFTSMC generates less chattering during the control process, thus avoiding wear and tear of the actuator and reduction of energy efficiency caused by chattering. The torque diagram of NFTSMC is more stable than that of NTSMC. NFTSMC can still maintain stable torque output when facing parameter changes or external disturbances, which indicates that NFTSMC has better robustness. NFTSMC can maintain stable torque output in the face of parameter changes or external disturbances, which indicates that NFTSMC has better robustness.

## 5. CONCLUSIONS

This academic paper presents an exhaustive control paradigm for an upper limb exoskeleton rehabilitation robot, highlighting key factors for the safety and effectiveness of robot-assisted rehabilitation training. The proposed framework is based on a trajectory planning methodology that combines polynomial interpolation and the minimum-jerk model to ensure that the training reference trajectory is both smoothly switchable and close to natural human kinematics.

The control frame includes a motion-switching feature designed to facilitate a seamless transition between two modes of operation: standard motion and safety stop. This function is crucial for maintaining patient safety during training, as it significantly reduces the likelihood of abrupt changes, thereby minimizing the potential for discomfort or injury. The disturbance observer-based NFTSMC design method described in this paper is capable of accurately tracking the necessary joint angles, with the exoskeleton tracking error converging to zero

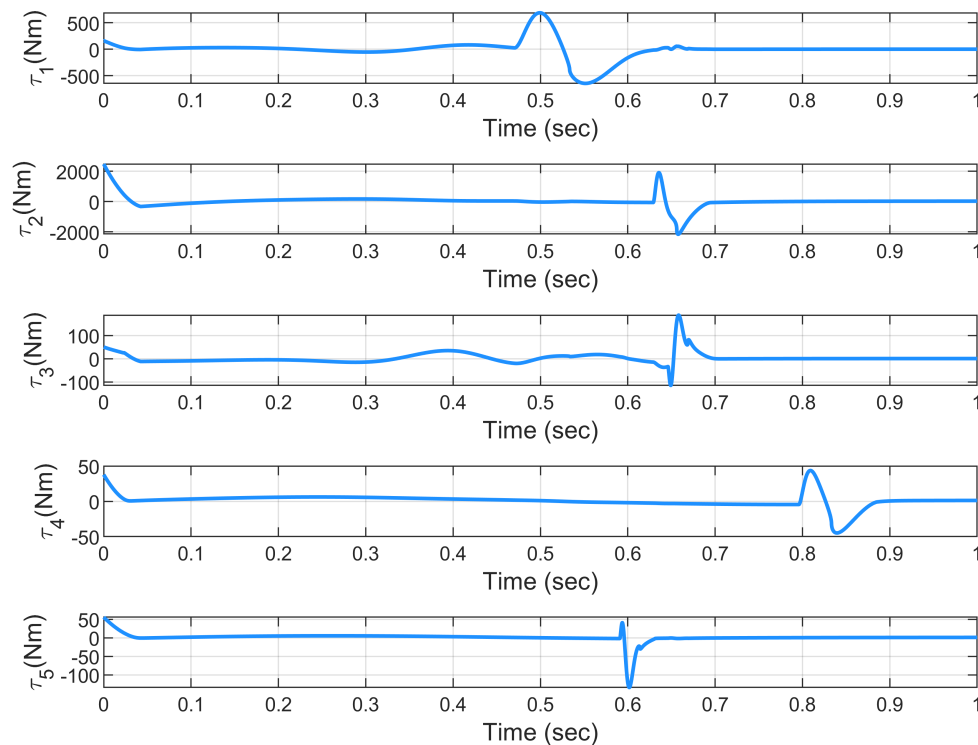


**Figure 14.** Control input in the case of NFTSMC. NFTSMC: Non-singular fast terminal sliding mode controller.

in a finite time frame. The robustness of this method to unknown bounded external perturbations advances and also solves the singularity problem and chattering phenomenon that often plague conventional slip-mode control systems.

The stability of the entire system is substantiated through the application of Lyapunov stability theory, providing a robust theoretical underpinning for the control framework. Simulation outcomes corroborate the efficacy and resilience of the proposed control framework, demonstrating its adaptability to variations in reference trajectories in response to safe mode settings and its capacity to maintain smooth operation with minimal chattering during modal transitions.

Whilst the current control framework has exhibited promising results, there exist realms for further refinement and development. One limitation highlighted in this discourse is the scheme's sensitivity to the initial state of the system. Future research endeavors will concentrate on mitigating this issue by incorporating fixed-time control strategies that can accommodate system model uncertainty. This will be instrumental in enhancing the robustness of the exoskeleton system, particularly in unpredictable real-world scenarios where initial conditions may exhibit significant variability. Another avenue for future inquiry is the enhancement of the motion-dependent switching function. Although the current function permits smooth modal transitions, there is potential to further optimize this function to respond more dynamically to alterations in patient movement and external conditions. This could entail the integration of sophisticated sensor technologies and machine learning algorithms to anticipate and adapt to patient requirements in real time. Furthermore, the integration of haptic feedback and virtual reality technologies into the exoskeleton system could engender a more immersive and engaging training experience for patients. This would not only augment the efficacy of the rehabilitation process but also bolster patient adherence to the training regimen.

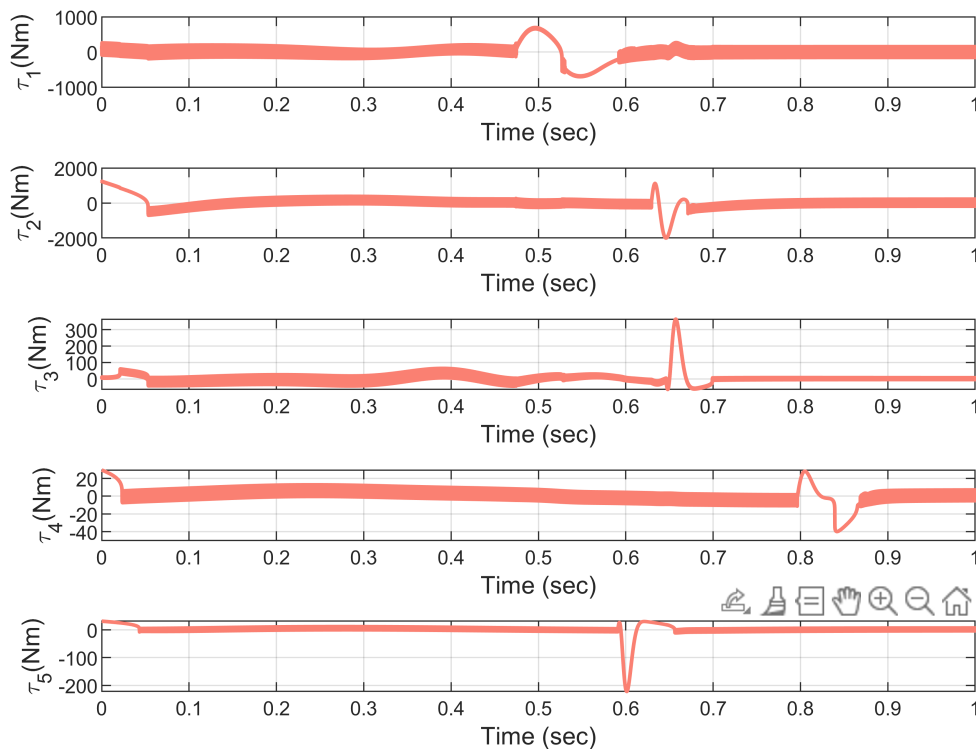


**Figure 15.** Control input in the case of NTSMC. NTSMC: Non-singular terminal sliding mode control.

In summation, this discourse establishes a solid foundation for the development of a stable and efficacious control framework for exoskeletal rehabilitation robots. Whilst the current framework has demonstrated efficacy in simulation, there are myriad opportunities for future research to build upon these findings and address the limitations identified. The ultimate objective is to create a system that not only enhances the physical rehabilitation of patients but also elevates their overall quality of life through a more personalized and engaging rehabilitation experience.

## DECLARATIONS

### Authors' contributions

Made substantial contributions to the conception and design of the study and performed data analysis and interpretation: Zhang, Y.

Performed data acquisition and provided administrative, technical, and material support: Xie, W.; Ma, R.

### Availability of data and materials

The data involved in this study are private and confidential due to privacy and confidentiality concerns. Therefore, we declare that the data will not be made publicly available. However, readers who require further information may contact the corresponding author to obtain the relevant data.

### Financial support and sponsorship

None.

### Conflicts of interest

All authors declared that there are no conflicts of interest.

**Ethical approval and consent to participate**

Not applicable.

**Consent for publication**

Not applicable.

**Copyright**

© The Author(s) 2025.

**REFERENCES**

1. Thayabaranathan, T.; Kim, J.; Cadilhac, D. A.; et al. Global stroke statistics 2022. *Int. J. Stroke.* **2022**, *17*, 946–56. [DOI](#)
2. Feigin, V. L.; Forouzanfar, M. H.; Krishnamurthi, R.; et al. Global and regional burden of stroke during 1990–2010: findings from the Global Burden of Disease Study 2010. *Lancet* **2014**, *383*, 245–54. [DOI](#)
3. Peng, L.; Hou, Z. G.; Peng, L.; Luo, L.; Wang, W. Robot assisted rehabilitation of the arm after stroke: prototype design and clinical evaluation. *Sci. China Inf. Sci.* **2017**, *60*, 073201. [DOI](#)
4. Bütetfisch, C.; Hummelsheim, H.; Denzler, P.; Mauritz, K. H. Repetitive training of isolated movements improves the outcome of motor rehabilitation of the centrally paretic hand. *J. Neurol. Sci.* **1995**, *130*, 59–68. [DOI](#)
5. Lum, P. S.; Bugar, C. G.; Shor, P. C.; Majmundar, M.; Van der Loos, M. Robot-assisted movement training compared with conventional therapy techniques for the rehabilitation of upper-limb motor function after stroke. *Arch. Phys. Med. Rehabil.* **2002**, *83*, 952–9. [DOI](#)
6. Norouzi-Gheidari, N.; Archambault, P. S.; Fung, J. Effects of robot-assisted therapy on stroke rehabilitation in upper limbs: systematic review and meta-analysis of the literature. *J. Rehabil. Res. Dev.* **2012**, *49*, 479–96. [DOI](#)
7. Sankar, K.; Muthukumar, S. D.; Kannan, P.; Mariappan, S.; Kalidoss, S. Robot-assisted therapies for upper limb stroke rehabilitation: a narrative review. *2024 International Conference on Cognitive Robotics and Intelligent Systems (ICC - ROBINS)*, Coimbatore, India. Apr 17–19, 2024. IEEE, 2024; pp. 750–6. [DOI](#)
8. Li, G.; Fang, Q.; Xu, T.; Zhao, J.; Cai, H.; Zhu, Y. Inverse kinematic analysis and trajectory planning of a modular upper limb rehabilitation exoskeleton. *Technol. Health Care.* **2019**, *27*, 123–32. [DOI](#)
9. Flash, T.; Meirovitch, Y.; Barliya, A. Models of human movement: trajectory planning and inverse kinematics studies. *Robot. Auton. Syst.* **2013**, *61*, 330–9. [DOI](#)
10. Wang, C.; Peng, L.; Hou, Z. G.; et al. Kinematic redundancy analysis during goal-directed motion for trajectory planning of an upper-limb exoskeleton robot. In: *2019 41st Annual International Conference of the IEEE Engineering in Medicine and Biology Society (EMBC)*, Berlin, Germany. Jul 23–27, 2019. IEEE, 2019; pp. 5251–5. [DOI](#)
11. Kim, H.; Miller, L. M.; Byl, N.; Abrams, G. M.; Rosen, J. Redundancy resolution of the human arm and an upper limb exoskeleton. *IEEE Trans. Biomed. Eng.* **2012**, *59*, 1770–9. [DOI](#)
12. Secco, E. L.; Visioli, A.; Magenes, G. Minimum jerk motion planning for a prosthetic finger. *J. Robot. Syst.* **2004**, *21*, 361–8. [DOI](#)
13. Ghobadi, M.; Sosnoff, J.; Kesavadas, T.; Esfahani, E. T. Using mini minimum jerk model for human activity classification in home-based monitoring. In: *2015 IEEE International Conference on Rehabilitation Robotics (ICORR)*, Singapore. Aug 11–14, 2015. IEEE, 2015. pp. 909–12. [DOI](#)
14. Zdravec, M.; Matjačić, Z. Development of optimization-based simulation tool for trajectory planning in planar arm reaching after stroke. In: *2012 4th IEEE RAS & EMBS International Conference on Biomedical Robotics and Biomechatronics (BioRob)*, Rome, Italy. Jun 24–27, 2012. IEEE, 2012. pp. 1446–50. [DOI](#)
15. Zdravec, M.; Matjačić, Z. Planar arm movement trajectory formation: An optimization based simulation study. *Biocybern. Biomed.* **2013**, *33*, 106–17. [DOI](#)
16. Friedman, J.; Flash, T. Trajectory of the index finger during grasping. *Exp. Brain. Res.* **2009**, *196*, 497–509. [DOI](#)
17. Averta, G.; Della Santina, C.; Valenza, G.; Bicchi, A.; Bianchi, M. Exploiting upper-limb functional principal components for human-like motion generation of anthropomorphic robots. *J. Neuroeng. Rehabil.* **2020**, *17*, 63. [DOI](#)
18. Li, Z.; Zuo, W.; Li, S. Zeroing dynamics method for motion control of industrial upper-limb exoskeleton system with minimal potential energy modulation. *Measurement.* **2020**, *163*, 107964. [DOI](#)
19. Huang, Y.; Jia, L.; Chen, J.; Zheng, J.; Guo, Y.; Tao, Y. A novel path planning algorithm considering the maximum deflection angle of joint. *IEEE Access.* **2021**, *9*, 115777–87. [DOI](#)
20. Wang, C.; Peng, L.; Hou, Z. G. A control framework for adaptation of training task and robotic assistance for promoting motor learning with an upper limb rehabilitation robot. *IEEE Trans. Syst. Man. Cybern. Syst.* **2022**, *52*, 7737–47. [DOI](#)
21. Chakravorty, S.; Kumar, S. Generalized sampling based motion planners with application to nonholonomic systems. In: *2009 IEEE International Conference on Systems, Man and Cybernetics*, San Antonio, USA. Oct 11–14, 2009. IEEE, 2009. pp. 4077–82. [DOI](#)
22. Bakaev, V. S.; Goloburkin, N. V.; Kulagin, K. A.; Anisimov, R. O. Trajectory planning of a manipulator robot in joints space. In: *2022 International Conference on Information, Control, and Communication Technologies (ICCT)*, Astrakhan, Russian Federation. Oct 03–07, 2022. IEEE, 2022. pp. 1–5. [DOI](#)
23. Sabbaghi, E.; Bahrami, M.; Ghidary, S. S. Learning of gestures by imitation using a monocular vision system on a humanoid robot. In:

- 2014 *Second RSI/ISM International Conference on Robotics and Mechatronics (ICRoM)*, Tehran, Iran. Oct 15-17, 2014. IEEE, 2014; pp. 588-94. [DOI](#)
24. Tang, S.; Chen, L.; Barsotti, M.; et al. Kinematic synergy of multi-DoF movement in upper limb and its application for rehabilitation exoskeleton motion planning. *Front. Neurobot.* **2019**, *13*, 99. [DOI](#)
  25. Shahbazi, H.; Parandeh, R.; Jamshidi, K. Implementation of imitation learning using natural learner central pattern generator neural networks. *Neural Netw.* **2016**, *83*, 94–108. [DOI](#)
  26. Lauretti, C.; Cordella, F.; Ciancio, A. L.; et al. Learning by demonstration for motion planning of upper-limb exoskeletons. *Front. Neurobot.* **2018**, *12*, 5. [DOI](#)
  27. Nguialem, C.; Raison, M.; Achiche, S. Motion planning of upper-limb exoskeleton robots: a review. *Appl. Sci.* **2020**, *10*, 7626. [DOI](#)
  28. Wu, Q.; Wang, X.; Chen, B.; Wu, H. Development of a minimal-intervention-based admittance control strategy for upper extremity rehabilitation exoskeleton. *IEEE Trans. Syst. Man. Cybern. Syst.* **2018**, *48*, 1005-16. [DOI](#)
  29. Li, X.; Yang, Q.; Song, R. Performance-based hybrid control of a cable-driven upper-limb rehabilitation robot. *IEEE Trans. Biomed. Eng.* **2021**, *68*, 1351-9. [DOI](#)
  30. Zhang, M.; Wang, C.; Zhang, C.; Li, P.; Liu, L. A unified switching control framework for continuous robot-assisted training. *IEEE/ASME Trans. Mechatron.* **2024**, *29*, 2743-55. [DOI](#)
  31. Wu, J.; Huang, J.; Wang, Y.; Xing, K.; Xu, Q. Fuzzy PID control of a wearable rehabilitation robotic hand driven by pneumatic muscles. In: *2009 International Symposium on Micro-NanoMechatronics and Human Science*, Nagoya, Japan. Nov 09-11, 2009. IEEE, 2009; pp. 408-13. [DOI](#)
  32. Proietti, T.; Jarrassé, N.; Roby-Brami, A.; Morel, G. Adaptive control of a robotic exoskeleton for neurorehabilitation. In: *2015 7th International IEEE/EMBS Conference on Neural Engineering (NER)*, Montpellier, France. Apr 22-24, 2015. IEEE, 2015; pp. 803-6. [DOI](#)
  33. Koshkouei, A. J.; Zinober, A. S. I. Terminal sliding mode control of MIMO linear systems. In: *Proceedings of the 2002 American Control Conference (IEEE Cat. No.CH37301)*, Anchorage, USA. May 08-10, 2002. IEEE, 2002; pp. 2106-11. [DOI](#)
  34. Feng, Y.; Yu, X.; Han, F. On nonsingular terminal sliding-mode control of nonlinear systems. *Automatica.* **2013**, *49*, 1715-22. [DOI](#)
  35. Zou, A. M.; Kumar, K. D.; Hou, Z. G.; Liu, X. Finite-time attitude tracking control for spacecraft using terminal sliding mode and Chebyshev neural network. *IEEE Trans. Syst. Man. Cyber. B.* **2011**, *41*, 950-63. [DOI](#)
  36. Kim, K. S.; Park, Y.; Oh, S. H. Designing robust sliding hyperplanes for parametric uncertain systems: a Riccati approach. *Automatica* **2000**, *36*, 1041-8. [DOI](#)
  37. Choi, H. H. LMI-based sliding surface design for integral sliding mode control of mismatched uncertain systems. *IEEE Trans. Autom. Control.* **2007**, *52*, 736-42. [DOI](#)
  38. Wen, C. C.; Cheng, C. C. Design of sliding surface for mismatched uncertain systems to achieve asymptotical stability. *J. Frankl. Inst.* **2008**, *345*, 926-41. [DOI](#)
  39. Utkin, V.; Shi, J. Integral sliding mode in systems operating under uncertainty conditions. In: *Proceedings of 35th IEEE Conference on Decision and Control*, Kobe, Japan. Dec 13, 1996. IEEE, 1996; pp. 4591-6. [DOI](#)
  40. Wei, X.; Zhang, H.; Guo, L. Composite disturbance-observer-based control and terminal sliding mode control for uncertain structural systems. *Int. J. Syst. Sci.* **2009**, *40*, 1009–17. [DOI](#)
  41. Man, Z.; Xing, H. Y. Terminal sliding mode control of MIMO linear systemst. *IEEE Trans. Circuits. Syst. I. Fundam. Theory. Appl.* **1997**, *44*, 1065-70. [DOI](#)
  42. Wang, C.; Zhang, Y.; Peng, L.; Zou, A. M.; Hou, Z. G. Dynamic modelling and adaptive control of an upper-limb robotic exoskeleton. In: *2024 IEEE International Conference on Advanced Information, Mechanical Engineering, Robotics and Automation (AIMERA)*, Wulumuqi, China. May 18-19, 2024. IEEE, 2024; pp. 249-54. [DOI](#)
  43. Hogan, N. An organizing principle for a class of voluntary movements. *J. Neurosci.* **1984**, *4*, 2745-54. [DOI](#)
  44. Yang, X. R.; Lin, X.; Yang, Y.; Zou, A. M. Finite-time attitude tracking control of rigid spacecraft with multiple constraints. *IEEE Trans. Aerosp. Electron. Syst.* **2024**, *60*, 3688-97. [DOI](#)
  45. Kang, H. B.; Wang, J. H. Adaptive control of 5 DOF upper-limb exoskeleton robot with improved safety. *ISA Trans.* **2013**, *52*, 844-52. [DOI](#)
  46. Yu, S.; Yu, X.; Shirinzadeh, B.; Man, Z. Continuous finite-time control for robotic manipulators with terminal sliding mode. *Automatica.* **2005**, *41*, 1957–64. [DOI](#)
  47. Feng, Y.; Yu, Y. H.; Han, F. L. On nonsingular terminal sliding-mode control of nonlinear systems. *Automatica.* **2013**, *49*, 1715-22. [DOI](#)